

# High-resolution image reconstruction using the Discontinuity Adaptive ICM algorithm

MARTINS, A.L.D. and MASCARENHAS, N.D.A.

Universidade Federal de São Carlos, Departamento de Computação  
Via Washington Luís, Km 235, CP 676, CEP: 13.565-905, São Carlos, SP, Brazil  
ana\_martins@dc.ufscar.br, nelson@dc.ufscar.br

## Abstract

*Super-Resolution reconstruction methods intend to reconstruct a high-resolution image from a set of low-resolution observations. For that, the observed images must have sub-pixel displacements between each other. This requirement allows the existence of different information on each of the low-resolution images. This paper discusses a Bayesian approach for the super-resolution reconstruction problem using Markov Random Fields (MRF) and the Potts-Strauss model for the image characterization. Since it is difficult to maximize the joint probability, the Iterated Conditional Modes (ICM) algorithm is used to maximize the local conditional probabilities sequentially. For the oversmoothness inherent to Maximum a Posteriori (MAP) formulations using MRF prior models, we adopt a discontinuity adaptive (DA) procedure for the ICM algorithm. The proposed method was evaluated in a simulated situation by the Peak signal-to-noise ratio (PSNR) method and the Universal Image Quality Index (UIQI). Also, video frames with sub-pixel displacements were used for the visual evaluation. The results indicate the effectiveness of our approach both by numerical and visual evaluation.*

## 1. Introduction

High-resolution images are usually necessary in a great number of applications: medical imaging; image surveillance methods; digital television picture technology; and high-precision classification in remote-sensing, just to name a few.<sup>1</sup> This kind of images can be acquired using high-resolution acquisition devices. However, there are several

cost and hardware limitations. For instance, the size of each detector of a charged-couple device (CCD) camera cannot be made arbitrarily small because of the shot noise effect [17]. Also, in positron emission tomography (PET) technology, besides the problem with the detector size, spatial resolution is limited by several factors such as patient motion and positron range of the isotope of interest [13]. Thus, it is of great interest to reconstruct a high resolution image using signal processing techniques. The super-resolution image reconstruction approach uses a set of low-resolution observations of the same scene to reconstruct an image in a high-resolution grid. For that, the low-resolution observations must have sub-pixel displacements between each other. This characteristic allows the existence of different information on each of the low-resolution images and the exceeding information can be used to increase the spatial resolution of the image. According to Park et al. [17], images with this characteristic can be acquired in many ways: from a single camera with several captures; from multiple cameras located in different positions; by scene motions or local objects movements; by vibrating imaging systems.

Tsai and Huang [20] were the first to address the problem of reconstructing a high-resolution image from a set of low-resolution observations of the same scene. They used a frequency domain approach based on the shifting property of the Fourier transform to model global translational scene motion. More recently, several algorithms were proposed to solve the same problem, most of them in a spatial domain context. In fact, despite the simplicity of frequency domain approaches, there are several disadvantages on this formulation [2]. For instance, it does not usually permit more general motion models. Spatial domain approaches allow arbitrary motion models, complex degradation models and, mainly, the inclusion of *a priori* constraints. Note that super-resolution reconstruction is considered an ill-posed problem. Thus, regularized solutions using *a priori* constraints are usually required. Several methods that follow this idea were proposed, including the following: projection onto convex sets (POCS) based

---

<sup>1</sup> This paper contains excerpts from the M.Sc. thesis named “Uso do Algoritmo ICM Adaptativo a Descontinuidades para o Aumento da Resolução de Imagens Digitais por Técnicas de Reconstrução por Super Resolução” by the first author. This research project was financially supported by CAPES.

approaches [19][24][22]; deterministic regularized methods [10][9][3]; and probabilistic reconstruction techniques imposing the prior probability density functions (MAP reconstruction methods) [18][8]. A remarkable point is that MAP formulations using MRF prior models are considered the most flexible and realistic approaches. Even under limited prior information, these formulations allow the imposition of usual images characteristics using just neighborhood relationships [2].

In the super-resolution context, there are usually only low-resolution noisy observations. Therefore, a common constraint to be imposed is smoothness. In a MAP-MRF approach, this constraint is expressed as the prior probability of the high-resolution image, which is uniquely determined by its local conditional probabilities [1]. Besides, in MRFs, only neighboring pixels have direct interaction. Thus, the smoothness constraint can be imposed just by considering that in a neighborhood the pixel values do not change abruptly. However, despite this facility, the maximization of the joint probability usually demand high computational power. Besides, the global optimization is difficult to be computed exactly and an approximation has to be used [15]. In this context, the ICM algorithm is an interesting alternative. It is a deterministic algorithm proposed by Besag [1], which maximizes the local conditional probabilities sequentially. A remarkable point about this algorithm is the very fast convergence rate. It is important to note that image models based on a MAP-MRF formulation usually implies uniform smoothness of the image. This oversmoothness do not respect discontinuities, where abrupt changes occur. Therefore, we adopt a DA procedure for the ICM algorithm. In this way, when a discontinuity is detected, the degree of interaction is adjusted not to smooth the area.

This work presents a coherent image formation model and a MAP-MRF approach for super-resolution image reconstruction using the DA ICM algorithm. We discuss the use of the Potts-Strauss model for the *a priori* probability density function of the high-resolution image.

The PSNR method and the UIQI were used for the numerical evaluation of the proposed approach in a simulated situation. Besides, video frames with sub-pixel displacements were used for the visual evaluation. The results indicate the considerable effectiveness of our approach. Section 2 discusses some super-resolution approaches. Section 3 briefly reviews some MRF concepts and the Potts-Strauss model. Section 4 presents the proposed method. Section 5 shows some results obtained in the simulation and in the real situation. Finally, Section 6 presents some discussions about the proposed method.

## 2. Super Resolution Reconstruction

The super-resolution image reconstruction methodology uses a set of low-resolution observations of the same scene to reconstruct a high-resolution image. It has proved to be useful in many practical situations in which high resolution images are required. In fact, super-resolution methods use signal processing techniques to obtain the high-resolution image. Thus, it overcomes the resolution limitation inherent to acquisition devices.

Each pair of low-resolution observations must present sub-pixel displacements between them. This requirement guarantees that each low-resolution image contains additional information that can be used to increase spatial resolution. If these displacements were multiples of the low-resolution pixel size, images would contain redundant information. Figure 1 illustrates two low-resolution grids with integer displacements between each other. Note that both images contain the same information. Images presenting sub-pixel displacements can be acquired from a single camera with several captures; from multiple cameras located in different positions; by scene motion or local object movements; by vibrating imaging systems; using video frames.

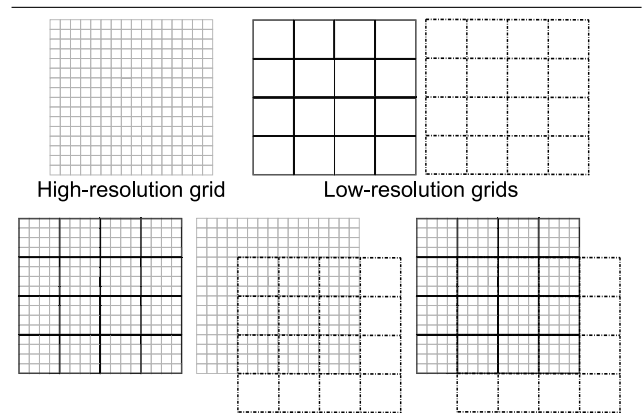


**Figure 1. Integer displacements between two low-resolution grids.**

According to Borman and Stevenson [2], the super-resolution methodology emerged from image interpolation methods applied for single frame resolution enhancement. As illustrated in Figure 2, more general problems have evolved from the actual methodology: spatial resolution enhancement of video sequences; temporal resolution enhancement of video sequences; and spatial-temporal resolution enhancement of video sequences. In this work we focus on the problem of reconstructing a high-resolution image, based on a set of low-resolution observations.

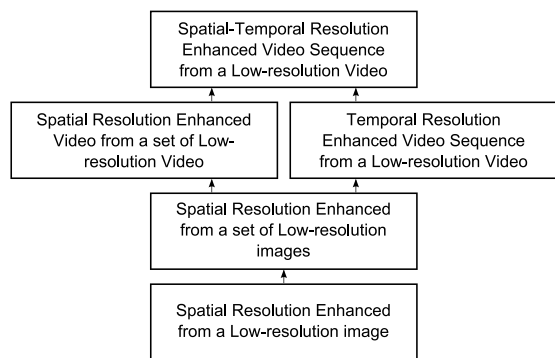


**Figure 2. The hierarchy of the spatial and temporal resolution enhancement techniques [2].**

Figure 3 illustrates the process of increasing the spatial resolution based on the observations. Note that to increase resolution, first of all it is necessary to identify the sub-pixel displacements among the low-resolution images. Image registration methods intend to map points in one image to the corresponding points in another image [4]. In this way, these images can be aligned with one another so that differences can be detected. Several sub-pixel image registration methods were proposed in the literature. For instance, Irani and Peleg [11] proposed a sub-pixel image registration and resolution enhancement method based on the back-projection procedure used in tomography; Xing et al. [23] proposed a multi-sensor and multi-resolution remote sensing image sub-pixel registration scheme; Guizar-Sicairos et al. [6] proposed a sub-pixel displacement estimation procedure based on the upsampled cross correlation of the reference image and each of the other observations.

Several algorithms were proposed in the last years for super-resolution image reconstruction [2][17]. In general,

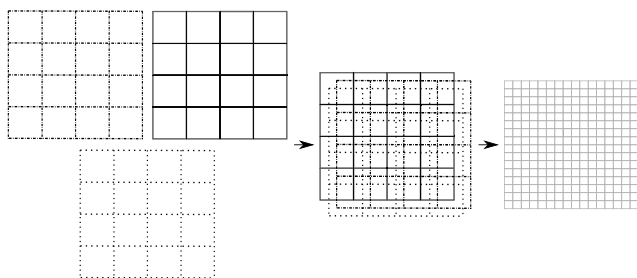


**Figure 3. Spatial resolution increased based on three low-resolution grids with sub-pixel displacements.**

they can be classified into two main classes: spatial and frequency domain approaches. Despite the simplicity of frequency domain approaches, they usually do not permit more general motion models. Spatial domain methods are able to work with more general observation models. Besides, they allow the inclusion of *a priori* constraints. In fact, there are usually only degraded observations and, besides increasing spatial resolution, super-resolution methods intend to reconstruct a high-quality digital image. In this sense, similar to restoration problems, super-resolution reconstruction is considered an ill-posed problem. Thus, some kind of regularization using *a priori* constraints is usually required.

POCS based approaches [19][24][22] impose prior knowledge by convex sets. This is a computational approach based on the theory that iterative projections onto convex sets converge to the intersection of all sets. In this way, given an initial estimation, the solution will respect all of the constraints represented by the sets. Despite the simplicity and flexibility of this approach, if the intersection of the sets is not a single point, there will be more than one solution. Thus, the result depends on the initial estimation. Besides, this approach demands high computational power. On the other hand, deterministic regularization methods use desired information about the solution to stabilize the inversion of the problem [10][9][3]. Smoothness is the most common constraint imposed. It assumes that, in general, images present limited high-frequency activity. However, in many cases, other priors would preserve high-frequency information in a better way. In this way, this approach models the prior information in an unfavorable way. It only includes a regularization term in the optimization function.

Probabilistic reconstruction techniques usually includes prior knowledge in a more natural way. The Bayesian MAP estimation is the most promising method. This approach uses the prior probability density function of the image to impose constraints to the solution. In this context, MRFs prior models are considered the most flexible and realistic because they allow the inclusion of images characteristics using only neighborhood relations.

### 3. Markov Random Fields

MAP formulations using MRF prior models are considered the most flexible and realistic approaches in the super-resolution context [2]. The MRF theory is based on contextual dependencies of physical phenomena. Let  $F = \{F_1, F_2, \dots, F_m\}$  be a set of random variables defined on a regular lattice  $S$ , and each  $F_i$  takes a value  $f_i \in L$ .  $(F_1 = f_1, F_2 = f_2, \dots, F_m = f_m)$  denotes the joint event that each  $F_i$  takes the value  $f_i, i = 1, \dots, m$ . In this way,  $F$  is called a random field and  $f = \{f_1, f_2, \dots, f_m\}$  is a realization of the field.

The sites in  $S$  are related by a neighborhood system  $\eta$ , defined by

$$\eta = \{\eta_i | \forall i \in S\}, \quad (1)$$

where  $\eta_i$  is the set of  $i$ 's neighbors. This neighborhood has the following properties:

1.  $i \notin \eta_i$ ;
2.  $i \in \eta_{i'} \iff i' \in \eta_i$ .

In the first order neighborhood system, every site has four neighbors. On the other hand, in the second order neighborhood system, every site has eight neighbors. Considering the site  $a$ , Figure 4 illustrates these neighborhood systems together with higher order systems indicated by the numbers in the third figure.

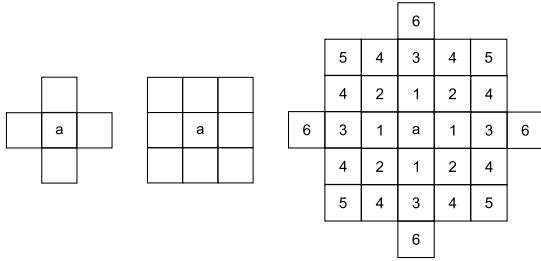


**Figure 4. Neighborhood systems on a regular lattice.**

A clique  $c$  is defined as a subset of sites in  $S$  that are neighbors to one another. Thus, it can consist of a single site  $c = i$ , a pair of sites  $c = i, i'$ , a triple of sites  $c = i, i', i''$ , and so on.

The collection of all cliques in a MRF is

$$C = C_1 \cup C_2 \cup C_3 \dots \quad (2)$$

where

$$C_1 = \{i | i \in S\}$$

$$C_2 = \{i, i' | i' \in \eta_i, i \in S\}$$

$$C_3 = \{i, i', i'' | i', i'' \in S \text{ are neighbors to one another}\}$$

and so on. In this way, considering the first order neighborhood system, the possible cliques are the first three cliques presented in Figure 5. The second order neighborhood system presents all the cliques showed in Figure 5.

For a discrete label set  $L$ ,  $P(f)$  denotes the joint probability of the realization  $f$ .  $F$  is called a MRF on  $S$  with respect to the neighborhood system  $\eta$ , if and only if

1.  $P(f) > 0, \forall f = \{f_1, f_2, \dots, f_m\}, f_i \in L$ ;
2.  $P(f_i | f_{S-\{i\}}) = P(f_i | f_{\eta_i})$ ,

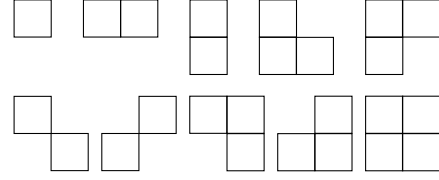


**Figure 5. Cliques on a regular lattice.**

where  $S - \{i\}$  is the set of sites in  $S$  without  $i$  and  $f_{S-\{i\}}$  is the set of labels of the sites in  $S - \{i\}$ .

The second property is called *Markovianity*. It depicts that in MRFs, only neighboring labels have direct interactions. In this way, a MRF is uniquely determined by its local conditional probabilities.

### 3.1. The MRF-Gibbs Equivalence

A random field  $F$  is said a Gibbs random field (GRF) on  $S$  according to  $\eta$ , if it is characterized by the Gibbs distribution

$$P(f) = Z^{-1} e^{-\frac{1}{T} U(f)} \quad (3)$$

where

$$Z = \sum_f e^{-\frac{1}{T} U(f)}. \quad (4)$$

$Z$  is called partition function, and the energy function  $U(f)$  is given by

$$U(f) = \sum_{c \in C} V_c(f), \quad (5)$$

where  $V_c(f)$  are the clique potentials that characterize the interaction between neighbors.

The Hammersley-Clifford theorem established the MRF-Gibbs equivalence [7]. It stated that  $F$  is a MRF on  $S$  according to a neighborhood system  $\eta$  if and only if  $F$  is a GRF on  $S$  according to  $\eta$ . This theorem provides a simple way of specifying the joint probability.

### 3.2. The Potts-Strauss Model

In general, since the Hammersley-Clifford theorem, the Gibbs distribution is adopted for the image characterization in MAP-MRF approaches. However, the maximization of the joint probability usually demand high computational power and the global optimization is difficult to be computed exactly. The Potts-Strauss model can be defined by the set of all the local conditional distributions  $p(f_i | f_{\eta_i})$ , which are defined as

$$p(f_i | f_{\eta_i}) \sim e^{\beta \sum_{t \in \eta_i: f_t = f_i} 1} \forall S \in S. \quad (6)$$

The parameter  $\beta$  is often referred to as the attraction or repulsion parameter whether it is positive or negative, respectively [16]. We believe the estimation process could be op-

timized by this model together with the maximization of the local conditional probabilities sequentially.

## 4. The Proposed Method

In a typical MAP reconstruction context, first of all it is necessary to formulate the image formation model that relates the desired high-resolution image to the low-resolution observations and the *a priori* distribution to be adopted. Also, for the sub-pixel displacements estimation, we must define how image registration will be applied.

### 4.1. Image Formation Model

Consider  $f[i, j]$ ,  $0 \leq i, j \leq M$ , the ideal undegraded image sampled above the Nyquist rate from the continuous scene of interest  $f : \mathbb{R}^2 \rightarrow \mathbb{R}$ . Following a lexicographic ordering of  $f[i, j]$ , an undersampled version  $d[k, l]$ ,  $0 \leq k, l \leq N$ ,  $N \leq M$ , can be modeled by

$$d = Df, \quad (7)$$

where  $D[u, v]$ ,  $0 \leq u \leq N^2$  and  $0 \leq v \leq M^2$ , is the down-sampling operator. In this sense, a low-resolution pixel is modeled as a weighted sum of the high-resolution pixels, in which the weights are given by the elements of operator  $D$ . Note that, according to the position of the acquisition sensors, this operator can be responsible for the presence of sub-pixel displacements among the low-resolution observations. As illustrated in Figure 6, the second low resolution grid is displaced from the previous grid by a fraction of the low-resolution pixel dimension in both horizontal and vertical directions.

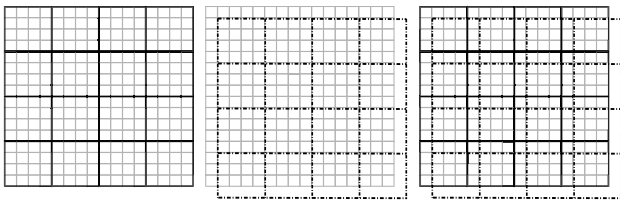


**Figure 6. Sub-pixel displacements caused by the downsampling operator.**

In a realistic situation, the digital image is usually blurred by the optical system during acquisition and also corrupted by noise. The blurring operator is often considered a linear space-invariant operator  $H$ , which elements are given by samples of the optical system point spread function (PSF). Thus, the blurred low-resolution image  $b$  is

given by  $b = Hd$  and  $H$  is a  $N^2 \times N^2$  block-circulant matrix. In this sense, a low resolution degraded version of the high-resolution image  $f$ , can be modeled by

$$g = HDf + n, \quad (8)$$

where  $n$  is additive noise.

### 4.2. Image Registration

The proposed method uses an initial high-resolution estimation to perform super-resolution reconstruction. This estimation can be derived according to the sub-pixel displacements between the low-resolution observations. Note that, in the alignment of the low resolution images with the high-resolution grid, several low-resolution pixels lay over one high-resolution pixel. Figure 7 illustrates the superposition of two low-resolution pixels over a fixed high-resolution pixel. Thus, in an intuitive way, each high-resolution pixel can be modeled as a composition of the low-resolution pixels influencing it. In this context, we implement the high-resolution pixel as a weighted sum of each low-resolution pixel that lay over it. The weights are defined according to the position of the high-resolution pixel under the low-resolution one.

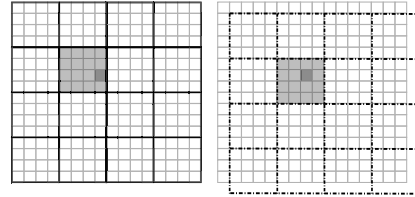


**Figure 7. Low resolution pixels that lay over a fixed high-resolution pixel.**

Figure 8 illustrates six of sixteen simulated images formed undersampling the a high-resolution image by four in each direction, each time starting from a different pixel within the first 4x4 block [19]. In this way, the low-resolution simulated images present sub-pixel displacements between each other. Figure 9 shows a 256x256 image used for this purpose (a); one of the 64x64 low-resolution simulated images (b); the high-resolution image reconstructed modeling each high-resolution pixel as a weighted sum of the low-resolution pixels that lay over it (c); and the bilinear interpolation of the low-resolution image (d).

For the sub-pixel displacements estimation, all observed images are compared with a reference image  $g_0(x, y)$ . The displacements  $x_0$  and  $y_0$  are estimated by minimizing the

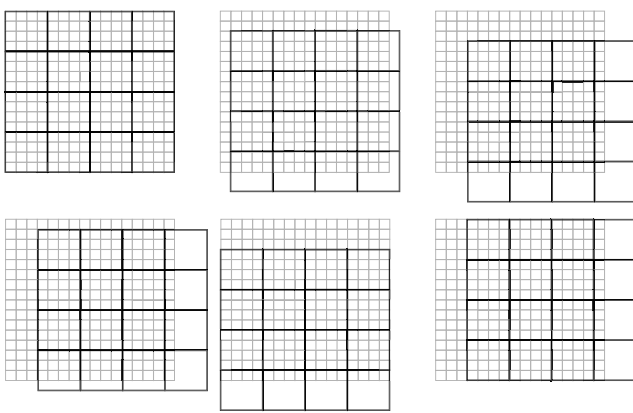


Figure 8. Six low-resolution simulated grids.

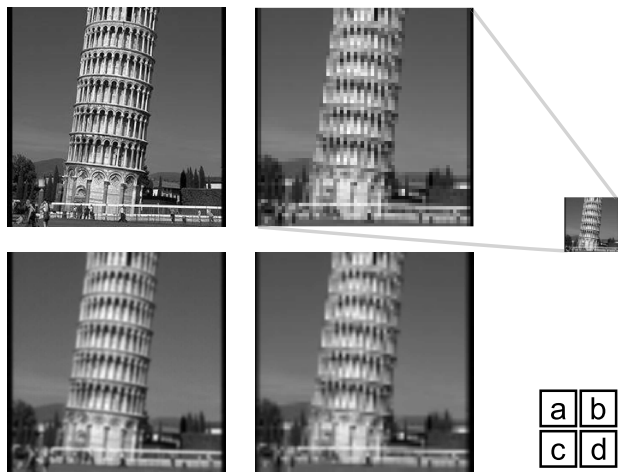


Figure 9. High-resolution image used to simulate sixteen low-resolution observations (a); first simulated image (b); reconstructed image (c); and bilinear interpolation of the low-resolution image (d).

similarity function

$$s(x_0, y_0) = \sum_{x \in X} \sum_{y \in Y} [g_0(x, y) - g_1(x - x_0, y - y_0)]^2, \quad (9)$$

where  $X$  and  $Y$  are finite sets of points.

Expanding  $g_1(x, y)$  to the first term of its Taylor series, it is easy to show that  $x_0^*$  and  $y_0^*$  that minimize Equation (9) are given by

$$x_0^* = \frac{\sum_x \sum_y [(g_0 - g_1)(x, y) - x_0^* g_{1x}(x, y)] g_{1x}(x, y)}{\sum_x \sum_y g_{1x}^2(x, y)} \quad (10)$$

and

$$y_0^* = \frac{\sum_x \sum_y [(g_0 - g_1)(x, y) - x_0^* g_{1x}(x, y)] g_{1y}(x, y)}{\sum_x \sum_y g_{1y}^2(x, y)} \quad (11)$$

where  $g_{1x}(x, y)$  and  $g_{1y}(x, y)$  are the first derivatives of  $g_1(x, y)$  in relation to  $x$  and  $y$ , respectively. This method only considers a set of globally translated and low-resolution observations. However, this assumption has been proved not to be so restrictive since we are considering very slight displacements between the images [11].

### 4.3. Bayesian Formulation for Super-Resolution

It is well known that high-resolution image reconstruction is an ill-posed problem. Thus, some kind of regularization is required to reach a good approximation of the original scene. In fact, a high-resolution estimation,  $\hat{f}$ , must be reconstructed considering a set of low-resolution observations  $g_k$ ,  $k = 1, \dots, q$ , each of them modeled by Equation (8). A Bayesian formulation usually provides a flexible and realistic way of imposing *a priori* constraints to the estimation. In this sense, the prior information is expressed as the prior probability of the high-resolution image and the MAP solution decides for the estimation that maximizes the conditional probability density of  $f$  given all the observations,

$$\hat{f} = \arg \max_f \{p(f|g)\}, \quad (12)$$

where  $g$  is composed by all of the low-resolution observations  $g_k$ ,  $k = 1, 2, \dots, q$ .

### 4.4. The Discontinuity Adaptive Approach

MAP-MRF formulations usually imply a uniform smoothness of the image. According to Li [14], since Geman and Geman [5] introduced the *line fields* idea, the application of the smoothness constraint while preserving discontinuities has been an active research issue in the image processing context. Discontinuity adaptive methods control the interaction between neighbors in such a way that the degree of interaction is adjusted when a discontinuity is detected.

The discontinuity detection is performed by an adaptive interactive function (AIF). Let  $k$  be the difference between a pixel and each of its neighbors. According to the value of this difference, the AIF has to distinguish noise from the presence of a discontinuity. For that, this function is convex in the interval  $[-B, B]$ , increasing monotonically with  $k$  to smooth out the noise. Outside this interval, the function is non-convex, decreasing as  $k$  increases and becoming zero as  $k \rightarrow \infty$  [14].

We adopt an AIF parameterized by  $\gamma$  given by

$$A_\gamma(x) = \gamma - \frac{\gamma}{1 + \frac{x^2}{\gamma}}, \quad (13)$$

which is convex in the interval  $B_\gamma = (-\sqrt{\frac{\gamma}{3}}, \sqrt{\frac{\gamma}{3}})$ . Figure 10 shows the qualitative shape of the adopted AIF function.

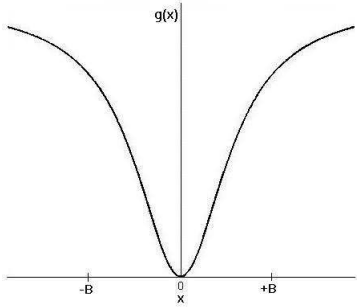


Figure 10. AIF adopted to the discontinuities detection.

#### 4.5. The Discontinuity Adaptive ICM Algorithm

The Iterated Conditional Modes algorithm was proposed by Besag [1] as a computationally feasible alternative for the MAP estimation. It uses a *greedy* strategy to maximize the local probabilities sequentially. The method is based on the local posterior distribution

$$p(f_i|g, f_{\eta_i}) \sim p(g_i|f_i) \cdot p(f_i|f_{\eta_i}), \quad (14)$$

given the observations  $g$  and the current values in the neighborhood  $\eta_i$ . As discussed in Section 3.2, the Potts-Strauss model is adopted as the prior distribution  $p(f_i|f_{\eta_i})$ .

We assume that the conditional probability density function  $p(g_i|f_i)$  is given by

$$p(g_i|f_i) = \frac{1}{\sigma\sqrt{2\pi}} \cdot e^{-\frac{(g_i - m_i)^2}{2\sigma^2}}, \quad (15)$$

where  $g_i$  is the weighted sum of the low-resolution pixels that lay over the high-resolution pixel,  $m_i = \frac{1}{C} \left( \sum_{j \in \eta_i} f_j \right) + \frac{1}{C} f_i$  and  $C = \#\eta_i + 1$ .

In each iteration, the ICM algorithm updates  $f_i$  by the value that maximizes  $p(g_i|f_i) \cdot p(f_i|f_{\eta_i})$ , for each  $i \in S$ . In our DA formulation, first of all, the AIFs  $A_\gamma(i)$ , for all  $i \in S$ , are calculated. Then,  $p(g_i|f_i) \cdot p(f_i|f_{\eta_i})$  is maximized considering only the values  $i' \in \eta_i$  which  $A_\gamma(i')$  is close to  $A_\gamma(i)$ .

In this context, the DA ICM algorithm is given by:

1. Choose an initial high-resolution estimation;

2. For  $i$  from 1 to  $M^2$ , update  $f_i$  by one of the values  $i' \in \eta_i$  that maximizes

$$p(g_i|f_i)p(f_i|\hat{f}_{\eta_i})$$

and  $A_\gamma(i')$  is close to  $A_\gamma(i)$ .

3. Repeat item (2)  $\tau_{iter}$  times.

$\tau_{iter}$  is the maximum number of iterations.

We used the image reconstructed using the low-resolution observations as discussed in Section 4.2, as the initial high-resolution estimation.

## 5. Results

Peak signal-to-noise ratio (PSNR) method and the Universal Image Quality Index (UIQI) were used for the numerical evaluation of the proposed approach in a simulated situation. Besides, in a real situation, video frames with sub-pixel displacements were used for the visual evaluation.

### 5.1. Simulation Description

The proposed method was evaluated in a simulated situation where sixteen low-resolution images were generated according to the image formation model discussed on Section 4.1. The image adopted as the high-resolution image to be reconstructed was undersampled as discussed on Section 4.2. In this way, the simulated observations present sub-pixel displacements between each other. Then, the images were convolved with a 3x3 uniform rectangular kernel to simulate the blur due to the image process acquisition and corrupted by additive and independent Gaussian noise at 30 dB. Figure 11 shows the 512x512 high-resolution image used (a) and the reference 128x128 low-resolution observation (b).

Figure 12 shows the high-resolution registered image as discussed on Section 4.2 (a); the bilinear interpolation of the reference low-resolution image (b); the high-resolution estimation reconstructed using the proposed method without the DA procedure (c); and the result using the DA constraint (d). As one can see, the registration procedure is able to give better results when compared with the interpolated image. Although in this simulation we have knowledge of the actual displacements between each low-resolution image and the reference image, we have estimated the displacement values. We note that the proposed method for sub-pixel registration has demonstrated to be very accurate in all conducted experiments.

In the simulations, the algorithm was initialized with the registered image in Figure 12 and the  $\beta$  parameter in Equation (6) was found following the procedure proposed in [12] for the second order neighborhood system. Also, in this experiment we do not take into account the blur from the optical system in the restoration process. From the presented



**Figure 11. High-resolution image used in the simulation (a) and one of the low-resolution images (b).**

results, we can see that the algorithm was able to improve the quality of the initial high-resolution estimation. We also note that in most of the experiments, the algorithm had fast convergence rate, where 5 or 6 iterations were sufficient to produce good results.

The oversmoothness inherent to the MAP-MRF formulation can be identified by uniform areas in the image. Figure 13 shows a zoom of the image reconstructed without imposing the DA constraint (a) and the image reconstructed with the DA procedure (b). Note that the DA approach avoids the formation of uniform areas in the image, preserving the details.

We used the Universal Image Quality Index proposed by Wang and Bovik [21] for the numerical evaluation. This index is given by

$$Q = \frac{4\sigma_{f\bar{q}}\bar{f}\bar{q}}{(\sigma_f^2 + \sigma_q^2)[(\bar{f})^2 + (\bar{q})^2]}, \quad (16)$$

where  $q$  is the image to be compared with the original image  $f$  and

$$\bar{f} = \frac{1}{M} \sum_{i=1}^M f_i, \quad \bar{q} = \frac{1}{M} \sum_{i=1}^M q_i, \quad (17)$$

$$\sigma_f^2 = \frac{1}{M-1} \sum_{i=1}^M (f_i - \bar{f})^2, \quad (18)$$

$$\sigma_q^2 = \frac{1}{M-1} \sum_{i=1}^M (q_i - \bar{q})^2, \quad (19)$$

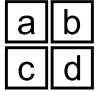


**Figure 12. Registered image used in the simulation (a); Bilinear interpolation of the reference low-resolution image (b); high-resolution estimation reconstructed without the DA procedure (c); and the result using DA constraint (d).**

$$\sigma_{fq} = \frac{1}{M-1} \sum_{i=1}^M (f_i - \bar{f})(q_i - \bar{q}). \quad (20)$$

$Q$  assumes values in the interval  $[-1, 1]$ . We believe this quality index is more appropriate to the super-resolution context since it models any distortion as a combination of three different factors: loss of correlation, luminance distortion, and contrast distortion.

Irani and Peleg's method [11], which presented the most important results in the super-resolution context, is used for comparison purpose. Since the proposed method does not include the deblurring process, the quality index was calculated using the blurred image as the original one. Table 1 shows the resulting quality indices. Indeed, the values shown are in agreement with a visual evaluation of the images. The proposed algorithm with the DA procedure presented a very similar evaluation compared with Irani and Peleg's method.

We also used the normalized mean squared error



Figure 13. Zoom of the image reconstructed without the imposition of the DA constraint (a) and the image reconstructed with the DA procedure (b).

(NMSE), given by

$$NMSE = \frac{\|f - q\|^2}{\|f\|^2} = \frac{\sum_{i=1}^M (f_i - q_i)^2}{\sum_{i=1}^M f_i^2} \quad (21)$$

to evaluate the same images. Table 1 shows that the results were very similar to the evaluation by the UIQI.

	UIQI	NMSE
Registered Image	0.9660	0.1439
ICM	0.9331	0.1709
DA ICM	0.9875	0.0577
Bilinear interpolation	0.9668	0.1445
Irani-Peleg	0.9897	0.0209

Table 1. UIQI and NMSE using the blurred image.

## 5.2. Case Study

In a real situation, we used video frames with sub-pixel displacements between each other to visual evaluate the proposed method. Figure 14 shows four 128x128 video frames. Considering the upsampling/downsampling factor 2, Figure 15 shows the 256x256 reconstructed image.

## 6. Concluding Remarks

We have presented an efficient algorithm for super-resolution image reconstruction based on a Markov random field where we used a DA procedure with the Iterated



Figure 14. Frames of a video, containing sub-pixel displacements between each other.

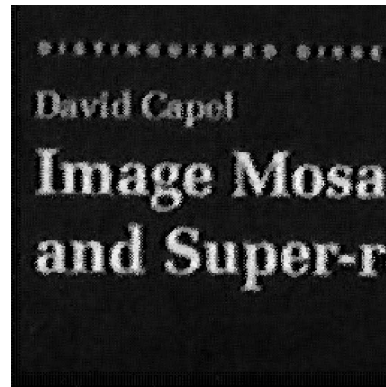


Figure 15. High-resolution reconstructed image.

Conditional Modes algorithm for computing the maximum *a posteriori* conditional probability. Indeed, the results demonstrate that the algorithm can be extremely efficient in a super-resolution reconstruction framework where the method has demonstrated good performance both in visual accuracy and computational cost. We also note that, although we do not address the image deblurring procedure in this work, it can be easily incorporated into the proposed algorithm. In future works, we intend to make additional experiments in order to verify the accuracy of the proposed method when compared with the Irani-Peleg algorithm and also considering different levels for the signal to noise ratio in the observations. We also intend to test the algorithm with other models for the *a priori* probability density function of the actual image.

## References

- [1] J. BESAG. Spatial interaction and the statistical analysis of lattice systems. *Journal of the Royal Statistical Society B*, 36(2):192–236, 1974.
- [2] J. L. BORMAN and R. STEVENSON. Spatial resolution enhancement of low-resolution image sequences - A comprehensive review with directions for future research. Technical report, University of Notre Dame, Notre Dame, IN, 1998.
- [3] N. K. BOSE, S. LERTRATTANAPANICH, and J. KOO. Advances in superresolution using L-curve. *Proc. Int. Symp. Circuits and Systems*, 2:433–436, 2001.
- [4] L. G. BROWN. A survey of image registration techniques. *ACM Computing Surveys*, 24(4):325–376, 1992.
- [5] S. GEMAN and D. GEMAN. Stochastic relaxation, Gibbs distribution, and the Bayesian restoration of images. *IEEE Transactions on Pattern Analysis and Machine Intelligence*, 6(6):721–741, 1984.
- [6] M. GUIZAR-SICAUIROS, S. T. THURMAN, and J. R. FIENUP. Efficient subpixel image registration algorithms. *Optics Letters*, 33(2):156–158, 2008.
- [7] J. M. HAMMERSLEY and P. CLIFFORD. Markov field on finite graphs and lattices. 1971.
- [8] R. C. HARDIE, K. J. BARNARD, and E. E. ARMSTRONG. Joint MAP registration and high-resolution image estimation using a sequence of undersampled images. *IEEE Trans. Image Processing*, 6:1621–1633, 1997.
- [9] R. C. HARDIE, K. J. BARNARD, J. G. BOGNAR, E. E. ARMSTRONG, and E. A. Watson. High-resolution image reconstruction from a sequence of rotated and translated frames and its application to an infrared imaging system. *Opt. Eng.*, 37(1):247–260, 1998.
- [10] M. C. HONG, M. G. KANG, and A. K. KATSAGGELOS. A regularized multichannel restoration approach for globally optimal high resolution video sequence. *SPIE VCIP*, 3024:1306–1317, 1997.
- [11] M. IRANI and S. PELEG. Improving resolution by image registration. *CVGIP: Graphical Models and Image Processing*, 53:231–239, 1991.
- [12] A. L. M. LEVADA, N. D. A. MASCARENHAS, and A. TANNÚS. Pseudolikelihood Equations for Potts MRF Model Parameter Estimation on Higher Order Neighborhood Systems. *IEEE Geoscience and Remote Sensing Letters*, 5(3), 2008. (accepted for publication).
- [13] C. L. LEVIN and E. J. HOFFMAN. Calculation of positron range and its effect on the fundamental limit of positron emission tomography system spatial resolution. *Phys. Med. Biol.*, 44:781–799, 1999.
- [14] S. Z. LI. On discontinuity-adaptive smoothness priors in computer vision. *IEEE Transactions on Pattern Analysis and Machine Intelligence*, PAM-17(6):576–586, june 1995.
- [15] S. Z. LI, Y. H. HUANG, and J. S. FU. Convex MRF potential functions. *Proceedings of the IEEE International Conference on Image Processing*, 2:296–299, 1995.
- [16] N. D. A. MASCARENHAS and A. C. FRERY. SAR image filtering with the ICM algorithm. *International Geoscience and Remote Sensing Symposium*, pages 2185–2187, August 1994.
- [17] S. C. PARK, M. K. PARK, and M. G. KANG. Super-resolution image reconstruction: a technical overview. *IEEE Signal Processing Magazine*, 20(3):21–36, 2003.
- [18] R. R. SCHULTZ and R. L. STEVENSON. Improved definition image expansion. *Proceedings of the IEEE International Conference on Acoustics, Speech and Signal Processing*, 3:173–176, 1992.
- [19] H. STARK and P. OSKOU. High-resolution image recovery from image-plane arrays, using convex projections. *Journal of Optical Society America A*, 6(11):1715–1726, 1989.
- [20] R. Y. TSAI and T. S. HUANG. Multi-frame image restoration and registration. *Advances in Computer Vision and Image Processing*, pages 317–339, 1984.
- [21] Z. WANG and A. C. BOVIK. A Universal Image Quality Index. *IEEE Signal Processing Letters*, 9(3):81–84, 2002.
- [22] F. WHEELER, R. HOCTOR, and E. BARRETT. Super-resolution image synthesis using projections onto convex sets in the frequency domain. In *Computational Imaging III. Edited by Bouman, Charles A.; Miller, Eric L. Proceedings of the SPIE*, volume 5674, pages 479–490, 2005.
- [23] S. XING, Q. XU, and D. MA. Multi-sensor Satellite Image Sub-pixel Registration. *Fourth International Conference on Image and Graphics, ICIG 2007*, pages 713–718, 2007. IEEE Computer Society.
- [24] S. YEH and H. STARK. Iterative and One-step Reconstruction from Nonuniform Samples by Convex Projections. *Journal of the Optical Society of America A*, 7:491–499, 1990.